

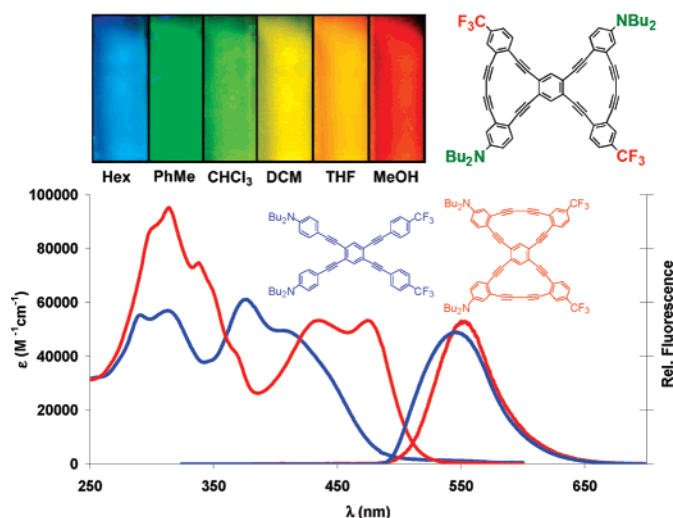
Structure–Property Relationships of Fluorinated Donor/Acceptor Tetrakis(phenylethynyl)benzenes and Bis(dehydrobenzoannuleno)benzenes

Eric L. Spitler, John M. Monson, and Michael M. Haley*

Department of Chemistry and Materials Science Institute, University of Oregon,
Eugene, Oregon 97403-1253

haley@uoregon.edu

Received November 27, 2007



Nine new bisdonor/bisacceptor-functionalized tetrakis(phenylethynyl)benzene (TPEB) and six new bis-(dehydrobenzoannuleno)benzene (DBA) chromophores have been synthesized. The compounds consist of electron-donating dibutylaniline groups connected through a conjugated phenyl–acetylene scaffold to benzotrifluoride, bis(trifluoromethyl)phenyl, or pentafluorophenyl acceptor groups. In comparison to previously reported analogues utilizing nitrophenyl or benzonitrile acceptor groups, the weaker acceptor groups exhibit visibly fluorescent intramolecular charge transfer (ICT) behavior, moderately narrow optical band gaps, moderately high quantum yields, and strong fluorescence solvatochromism. In this series of molecules, the strongly inductive fluoro acceptor groups result in optical properties similar to the resonance acceptor analogues, making them promising candidates for optical materials device components. The data also support recent investigations that question the utility of using UV/vis spectroscopy alone as a qualitative measure of conjugation. The bisDBAs exhibit weaker ICT behavior and self-association in solution than their corresponding nitro analogues, but show greater stability to decomposition via polymerization and smaller optical band gaps than their acyclic analogues.

Introduction

Donor/acceptor-substituted tetrakis(phenylethynyl)benzenes (TPEBs)¹ are two-dimensional, carbon-rich chromophores² which exhibit a high degree of conjugation, and consequently

possess multiple pathways for intramolecular electronic and photonic transfer. These cruciform-shaped molecules exhibit spatial separation of their frontier molecular orbitals, making TPEBs excellent candidates for a variety of advanced materials applications, such as organic light-emitting diodes, thin film organic transistors, solar cells, and optical storage devices.^{3–5} Carbon-rich cruciforms already possess demonstrated potential

* Address correspondence to this author. Fax: 541-346-0487. Phone: 541-346-0456.

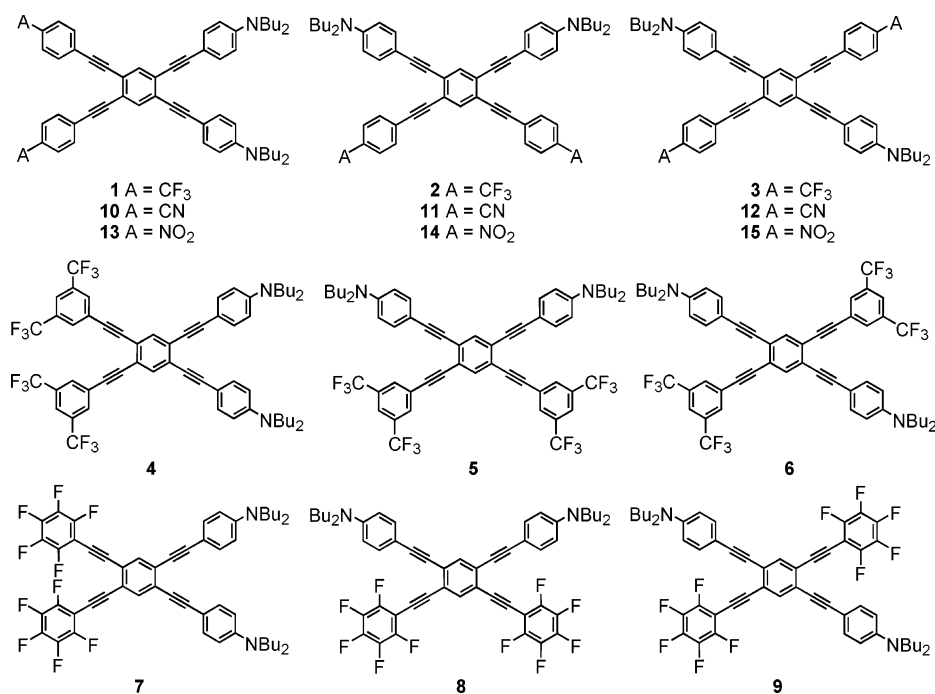


FIGURE 1. Target donor/acceptor TPEBs **1–9** with benzotrifluoride and perfluorophenyl acceptor units, and known nitrophenyl and benzonitrile acceptor TPEBs **10–15**.

as nonlinear optical/two-photon absorption⁶ and fluorescent sensing materials.⁷

Our previous studies have focused on the syntheses and spectroscopic characteristics of bisdonor/bisacceptor TPEBs incorporating dibutylaniline groups as the donor groups and nitrophenyl,^{1a,b} pyridyl,^{1c} or benzonitrile^{1a,d} groups as the acceptors. We showed that adjusting the identity of the acceptor group and topology of the chromophore led to predictable variations in the electronic absorption and emission profiles. These small structural variations allow fine-tuning of optical band gap energies and emissive wavelengths for customized optical materials applications. To date though, we have not examined inductive accepting groups that participate in charge transfer through the σ -framework only.⁸ Such structures may display similar optical behavior, but with greater chemical stability or bulk processing characteristics. Herein we describe further studies in acceptor group variation with the addition of benzotrifluoride- and pentafluorophenyl-functionalized donor/acceptor TPEBs (**1–9**, Figure 1) and the impact of the variations on the optical properties. Of particular interest is comparison of the properties of the inductive fluoro-accepting groups of **1–9** to those of the nitrile (**10–12**) and nitro (**13–15**) resonance

acceptors. By undertaking parallel investigations of chromophores with both one (**1–3**) and two (**4–6**) trifluoromethyl groups per acceptor arene, we can also evaluate the cumulative effect of the number of acceptors per arene ring. Since the electron withdrawal is through-bond only, the position of the $-\text{CF}_3$ groups relative to the acetylene bridge should have little

(3) Reviews, inter alia: (a) *Functional Organic Materials*; Müller, T. J. J., Bunz, U. H. F., Eds.; Wiley-VCH: Weinheim, Germany, 2007. (b) *Organic Light Emitting Devices: Synthesis Properties and Applications*; Mullen, K., Scherf, U., Eds.; Wiley-VCH: Weinheim, Germany, 2006. (c) Chen, J.; Reed, M. A.; Dirk, S. M.; Price, D. W.; Rawlett, A. M.; Tour, J. M.; Grubisha, D. S.; Bennett, D. W. In *NATO Science Series II: Mathematics Physics Chemistry (Molecular Electronics: Bio-Sensors and Bio-Computers)*; Plenum: New York, 2003; Vol. 96, pp 59–195. (d) Shirota, Y. *J. Mater. Chem.* **2000**, *10*, 1–25. (e) Schwab, P. F. H.; Levin, M. D.; Michl, J. *Chem. Rev.* **1999**, *99*, 1863–1933. (f) *Electronic Materials: The Oligomer Approach*; Müllen, K., Wegner, G., Eds.; Wiley-VCH: Weinheim, Germany, 1998. (g) *Nonlinear Optics of Organic Molecules and Polymers*; Nalwa, H. S., Miyata, S., Eds.; CRC Press: Boca Raton, FL, 1997.

(4) Recent examples, inter alia: (a) Kang, H.; Evrenenko, G.; Dutta, P.; Clays, K.; Song, K.; Marks, T. J. *J. Am. Chem. Soc.* **2006**, *128*, 6194–6205. (b) Knox, J. E.; Halls, M. D.; Hrachian, H. P.; Schlegel, H. B. *Phys. Chem. Chem. Phys.* **2006**, *8*, 1371–1377. (c) Shukla, V. K.; Kumar, S.; Deva, D. *Synth. Met.* **2006**, *156*, 387–391. (d) Seminario, J. M. *Nat. Mater.* **2005**, *4*, 111–113. (e) Hughes, G.; Bryce, M. R. *J. Mater. Chem.* **2005**, *15*, 94–107. (f) Van der Auweraer, M.; De Schryver, F. C. *Nat. Mater.* **2004**, *3*, 507–508. (g) Special Issue on Organic Electronics. *Chem. Mater.* **2004**, *16*, 4381–4846. (h) Simpson, C. D.; Wu, J.; Watson, M. D.; Müllen, K. *J. Mater. Chem.* **2004**, *14*, 494–504.

(5) Inter alia: (a) Zhao, Y.; Slepokov, A. D.; Akoto, C. O.; McDonald, R.; Hegmann, F. A.; Tykwinski, R. R. *Chem. Eur. J.* **2005**, *11*, 321–329. (b) Bunz, U. H. F. *Adv. Polym. Sci.* **2005**, *177*, 1–52. (c) Fasina, T. M.; Collings, J. C.; Lydon, D. P.; Albasa-Jove, D.; Batsanov, A. S.; Howard, J. A. K.; Nguyen, P.; Bruce, M.; Scott, A. J.; Clegg, W.; Watt, S. W.; Viney, C.; Marder, T. B. *J. Mater. Chem.* **2004**, *14*, 2395–2404. (d) Boydston, A. J.; Yin, Y.; Pagenkopf, B. L. *J. Am. Chem. Soc.* **2004**, *126*, 3724–3725. (e) Gonzalo-Rodríguez, J.; Esquivias, J.; Lafuente, A.; Diaz, C. *J. Org. Chem.* **2003**, *68*, 8120–8128. (f) Nielsen, M. B.; Diederich, F. In *Modern Arene Chemistry*; Astruc, D., Ed.; Wiley-VCH: Weinheim, Germany, 2002; pp 196–216. (g) Watson, M. D.; Fechtenkötter, A.; Müllen, K. *Chem. Rev.* **2001**, *101*, 1267–1300. (h) Tykwinski, R. R.; Gubler, U.; Martin, R. E.; Diederich, F.; Bosshard, C.; Günter, P. *J. Phys. Chem. B* **1998**, *102*, 4451–4465.

(1) (a) Miller, J. J.; Marsden, J. A.; Haley, M. M. *Synlett* **2004**, 165–168. (b) Marsden, J. A.; Miller, J. J.; Shirtcliff, L. D.; Haley, M. M. *J. Am. Chem. Soc.* **2005**, *127*, 2464–2476. (c) Spitler, E. L.; Shirtcliff, L. D.; Haley, M. M. *J. Org. Chem.* **2007**, *72*, 86–96. (d) Samori, S.; Tojo, S.; Fujitsuka, M.; Spitler, E. L.; Haley, M. M.; Majima, T. *J. Org. Chem.* **2007**, *72*, 2785–2793. (e) Spitler, E. L.; McClintock, S. P.; Haley, M. M. *J. Org. Chem.* **2007**, *72*, 6692–6699.

(2) (a) de Meijere, A., Ed. *Carbon Rich Compounds I*; Topics in Current Chemistry; Springer: Berlin, Germany, 1998; Vol. 196. (b) de Meijere, A., Ed. *Carbon Rich Compounds II*; Topics in Current Chemistry; Springer: Berlin, Germany, 1999; Vol. 201. (c) Diederich, F.; Stang, P. J.; Tykwinski, R. R., Eds. *Acetylene Chemistry: Chemistry Biology and Material Science*; Wiley-VCH: Weinheim, Germany, 2005. (d) Haley, M. M.; Tykwinski, R. R., Eds. *Carbon-Rich Compounds: From Molecules to Materials*; Wiley-VCH: Weinheim, Germany, 2006.

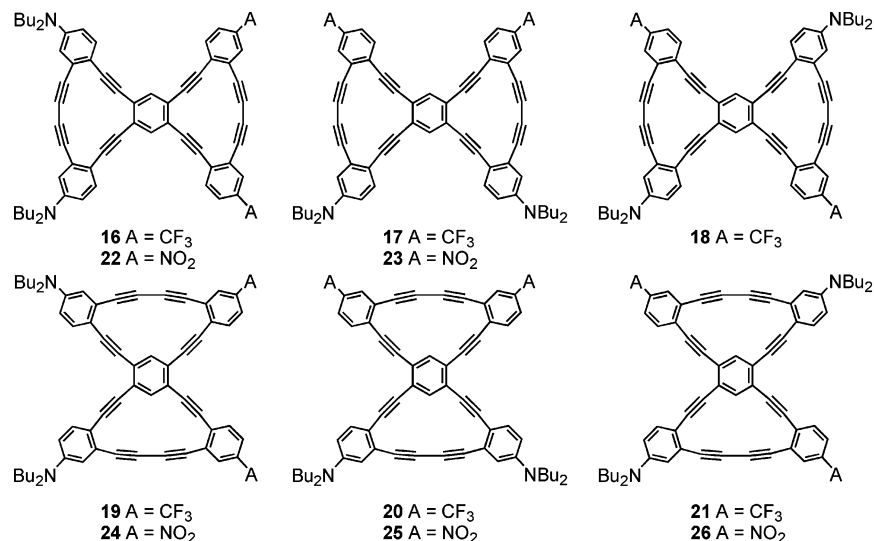


FIGURE 2. Target donor/acceptor DBAs **16–21** with dibutylaniline donors and trifluoromethyl acceptors and previously reported nitro-functionalized DBAs **22–26**.

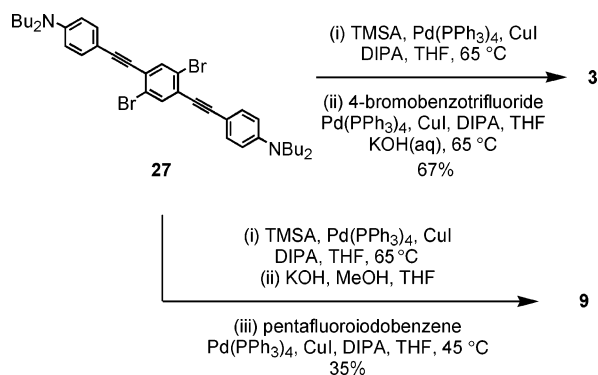
(if any) impact on the optical properties, allowing us to maintain symmetry and thus avoid dissimilar net dipole effects between isomers.

We have had a longstanding interest in the effects of enforced planarization on the photophysics and materials properties of phenyl–acetylene scaffolding.⁹ Accordingly, we also targeted bis(dehydrobenzo[14]- and [15]annuleno)benzene (bisDBA) macrocycle analogues of **1–3** (i.e., **16–21**, Figure 2), in an attempt to derive structure–property characteristics from comparison both to the acyclic variants as well as the previously reported nitro-functionalized DBAs (**22–26**).^{1b} In addition to planarization, **16–21** possess additional conjugated chromophore pathways, and [15]DBAs **19–21** contain a cross-conjugated pathway at the central arene.

Results and Discussion

Synthesis. Scheme 1 illustrates the modular synthesis of **1–9**. Trimethylsilylacetylene (TMSA) was cross-coupled¹⁰ to donor bromide **27**^{1c} at 65 °C, which was followed by an in situ deprotection/2-fold cross-coupling¹¹ of the acceptor haloarene. In this way, TPEBs **1–6** were prepared from only three key intermediates, similar to the ethynylpyridine analogues.^{1c} In the

SCHEME 1. Representative Syntheses of Donor/Acceptor TPEBs **3** and **9**



case of **7–9**, stepwise deprotection after TMSA coupling to **27** was necessary to avoid nucleophilic substitution of the fluorinated arenes by base generated under the in situ deprotection conditions (Scheme 1, bottom).^{7b,12} A complete listing of yields is given in Table 1.

BisDBAs **16–21** were prepared by the same general routes described for the nitro-functionalized analogues.^{1b,13} Donor and acceptor segments were synthesized separately and appended to the central arenes in a stepwise fashion. The differentially silylated bis-alkyne acceptor segment was prepared from

(6) (a) Slepko, A.; Marsden, J. A.; Miller, J. J.; Shirtcliff, L. D.; Haley, M. M.; Kamada, K.; Tykwinski, R. R.; Hegmann, F. A. *Proc. SPIE–Int. Soc. Opt. Eng.* **2005**, 5934, 29–34. (b) Slepko, A.; Hegmann, F. A.; Tykwinski, R. R.; Kamada, K.; Ohta, K.; Marsden, J. A.; Spitzer, E. L.; Miller, J. J.; Haley, M. M. *Opt. Lett.* **2006**, 31, 3315–3317. (c) Zhang, X.-B.; Feng, J.-K.; Ren, A.-M.; Sun, C.-C. *Opt. Mater.* **2007**, 29, 955–962. (d) See also: Kang, H.; Zhu, P.; Yang, Y.; Facchetti, A.; Marks, T. J. *J. Am. Chem. Soc.* **2004**, 126, 15974–15975.

(7) (a) Wilson, J. N.; Bunz, U. H. F. *J. Am. Chem. Soc.* **2005**, 127, 4124–4125. (b) Zuccherro, A. J.; Wilson, J. N.; Bunz, U. H. F. *J. Am. Chem. Soc.* **2006**, 128, 11872–11881. (c) McGrier, P. L.; Solntsev, K. M.; Schönhaber, J.; Brombosz, S. M.; Tolbert, L. M.; Bunz, U. H. F. *Chem. Commun.* **2007**, 2127–2129. (d) Hauck, M.; Schönhaber, J.; Zuccherro, A. J.; Hardcastle, K. L.; Muller, T. J. J.; Bunz, U. H. F. *Org. Chem.* **2007**, 72, 6714–6725. (e) Brombosz, S. M.; Zuccherro, A. J.; Phillips, R. L.; Vazquez, D.; Wilson, A.; Bunz, U. H. F. *Org. Lett.* **2007**, 9, 4519–4522.

(8) (a) Nguyen, P.; Todd, S.; van den Biggelaar, D.; Taylor, N. J.; Marder, T. B.; Wittman, F.; Friend, R. H. *Synlett* **1994**, 299–301. (b) Tolulope, M. F.; Collings, J. C.; Burke, J. M.; Batsanov, A. S.; Ward, R. M.; Albesa-Jove, D.; Porres, L.; Beeby, A.; Howard, J. A. K.; Scott, A. J.; Clegg, W.; Watt, S. W.; Viney, C.; Marder, T. B. *J. Mater. Chem.* **2005**, 15, 690–697.

(9) Inter alia: (a) Marsden, J. A.; Haley, M. M. *J. Org. Chem.* **2005**, 70, 10213–10226. (b) Miller, J. J.; Marsden, J. A.; Haley, M. M. *Angew. Chem., Int. Ed.* **2004**, 43, 1694–1697. (c) Marsden, J. A.; Palmer, G. J.; Haley, M. M. *Eur. J. Org. Chem.* **2003**, 2355–2369. (d) Haley, M. M. *Synlett* **1998**, 557–565.

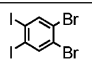
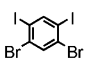
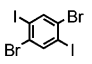
(10) (a) Marsden, J. A.; Haley, M. M. in *Metal Catalyzed Cross-Coupling Reactions*, 2nd ed.; de Meijere, A.; Diederich, F., Eds.; Wiley-VCH: Weinheim, Germany, 2004; pp 317–394. (b) Sonogashira, K. In *Metal-Catalyzed Cross-Coupling Reactions*; Diederich, F.; Stang, P. J., Eds.; Wiley-VCH: Weinheim, Germany, 1998; pp 203–230.

(11) (a) Haley, M. M.; Bell, M. L.; English, J. J.; Johnson, C. A.; Weakley, T. J. R. *J. Am. Chem. Soc.* **1997**, 119, 2956–2957. (b) Bell, M. L.; Chiechi, R. C.; Johnson, C. A.; Kimball, D. B.; Wan, W. B.; Weakley, T. J. R.; Haley, M. M. *Tetrahedron* **2001**, 57, 3507–3520.

(12) Brooke, G. M. *J. Fluorine Chem.* **1997**, 86, 1–76.

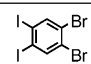
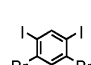
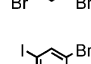
(13) (a) Pak, J. J.; Weakley, T. J. R.; Haley, M. M. *J. Am. Chem. Soc.* **1999**, 121, 8182–8192. (b) Sarkar, A.; Pak, J. J.; Rayfield, G. W.; Haley, M. M. *J. Mater. Chem.* **2001**, 11, 2943–2945.

TABLE 1. Yields for the Preparation of TPEBs 1–9

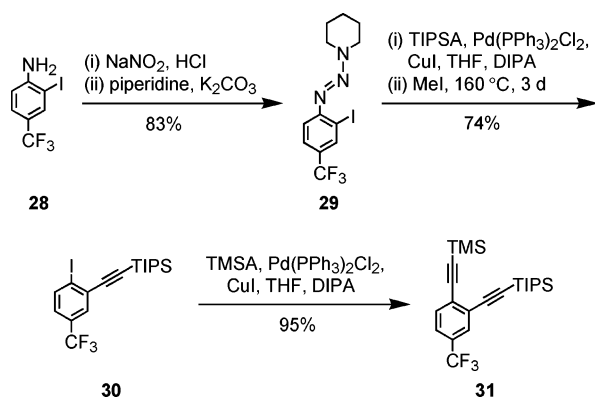
haloarerene	donor coupling ^a	TMSA/4-bromo-benzotrifluoride coupling (pdt)	TMSA/3,5-bis(trifluoromethyl)bromobenzene coupling (pdt)	TMSA/pentafluoriodobenzene coupling (pdt)
	70%	80% (1)	42% (4)	43% (7)
	89%	80% (2)	40% (5)	42% (8)
	89%	67% (3)	22% (6)	35% (9)

^a Reference 1c.

TABLE 2. Yields for the Preparation of DBAs 16–21

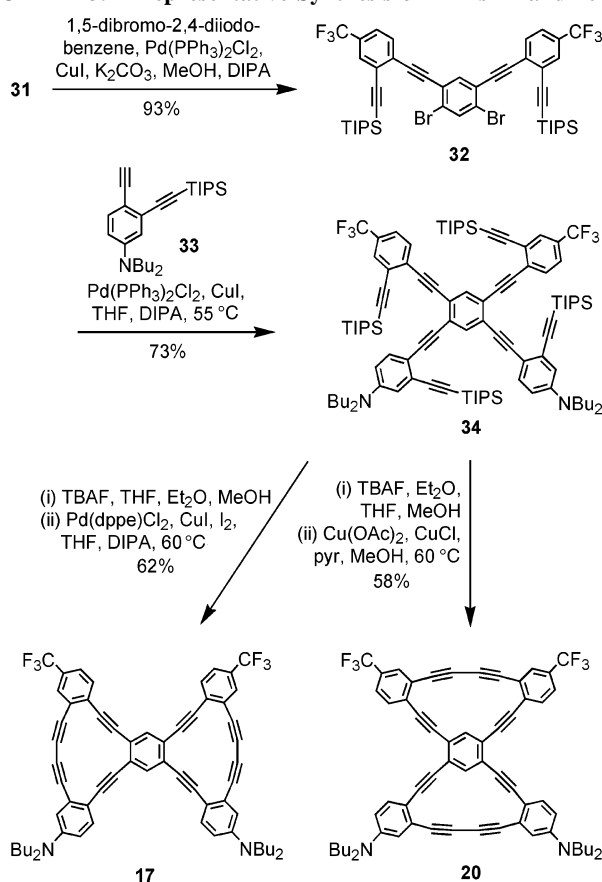
haloarerene	acceptor coupling	donor coupling	cyclization	bisDBA
	92%	18%	14%	16
	93%	73%	64%	19
	86%	37%	58%	20
			60%	21

SCHEME 2. Synthesis of Acceptor Segment 31



iodoaniline **28** (Scheme 2) first by conversion to triazene **29**. Sonogashira cross-coupling of triisopropylsilylacetylene (TIPSA) followed by displacement of the triazene at high temperature afforded iodoarene **30**. A second coupling of TMSA provided segment **31** in good overall yield. Selective deprotection of **31** under mildly basic conditions followed by coupling to isomers of dibromodiodobenzene furnished the acceptor-functionalized intermediates (e.g., **32**, Scheme 3). Cross-coupling of donor diyne **33**^{1b} at elevated temperature afforded the bisannulene precycles. Removal of the TIPS groups with TBAF followed by selective macrocyclization under either Pd- or Cu-mediated conditions gave the [14]- or [15]-membered bisDBAs, respectively.^{9b} For example, precycle **34** can be converted to either bisDBA **17** or **20**. Yields are given in Table 2. Compounds deriving from the 1,5-dibromo-2,4-diiodobenzene starting arene (the “meta” isomers) consistently proceeded in higher yields. This is likely due to the lack of steric hindrance during the 2-fold couplings as well as having withdrawing groups (bromo in the first case, acceptor segments in the second

SCHEME 3. Representative Synthesis of DBAs 17 and 20



case) para to the coupling site on the arene, since the Sonogashira reaction has a well-known preference for electron-poor arenes.¹⁰

Electronic Absorption Spectra. The electronic absorption spectra of TPEBs 1–9 in CH₂Cl₂ are shown in Figure 3, along

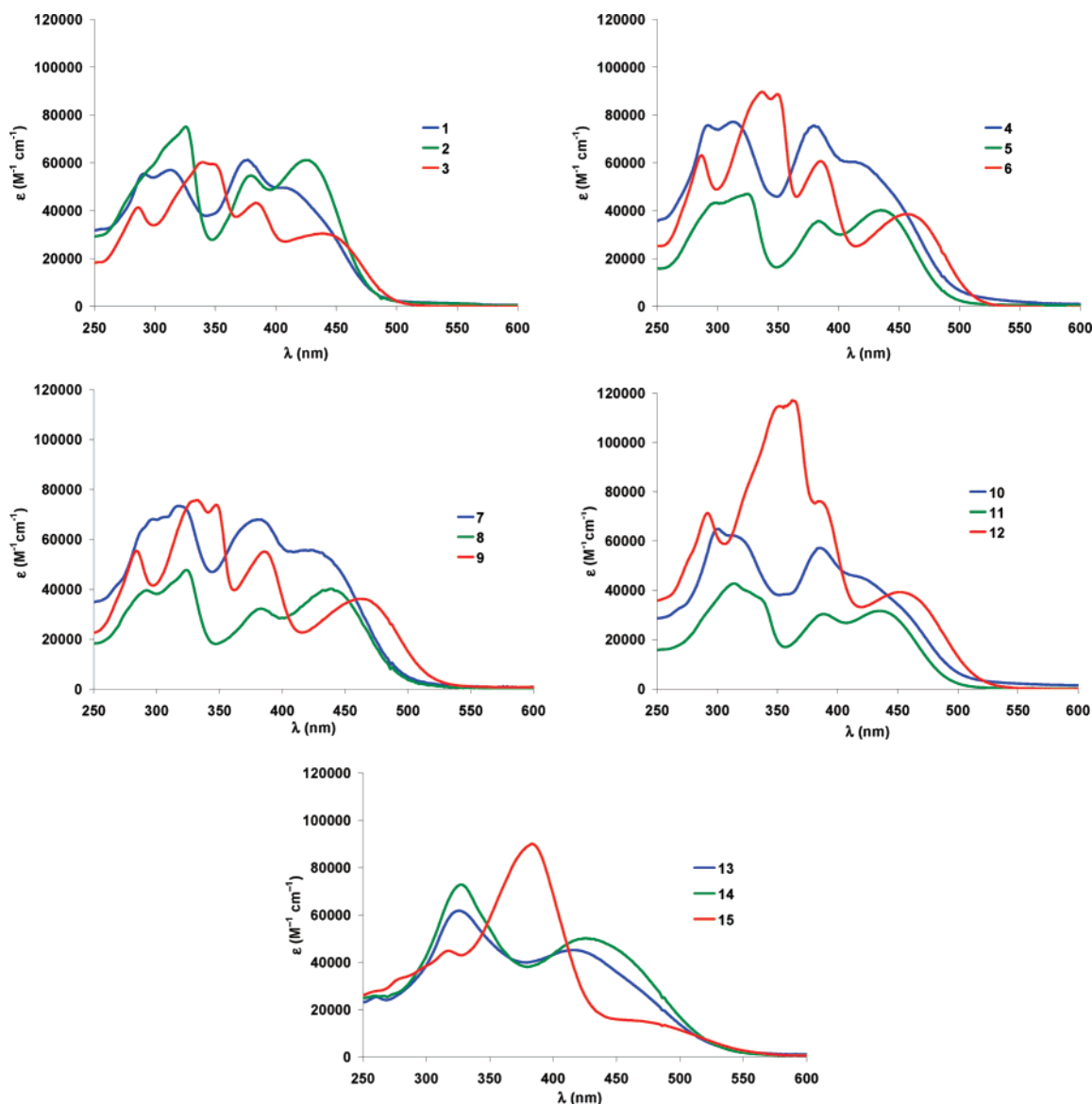


FIGURE 3. Electronic absorption spectra of (a) **1–3**, (b) **4–6**, (c) **7–9**, (d) **10–12**,^{1d} and (e) **13–15**.^{5,6} All spectra recorded in CH₂Cl₂ at analyte concentrations of 15–25 μ M.

with the spectra of known **10–15** for comparison.^{1a,b,d} Lowest energy bands, along with the emission data, are given in Table 3. The next higher bands are listed in the Supporting Information. All donor/acceptor-functionalized systems display a characteristic broad, low-intensity band in the 400–500 nm region with extinction coefficients of ca. 20000–60000 $\text{M}^{-1} \text{cm}^{-1}$, indicative of intramolecular charge transfer.^{1,13,14} Calculated molecular orbital plots for **13–15** and **22–26** show dramatic spatial separation of frontier molecular orbitals (FMOs) upon donor/acceptor functionalization.^{1b} Calculations of the FMOs of the ethynylpyridine analogues show similar but weakened charge-transfer polarization.^{1c} With this in mind, we expect the same properties in the cases of **1–9**. The trend in longest wavelength λ_{max} , which is correlated to the optical band gap, holds across the substitution isomers of each acceptor variant triad: isomers in which like groups are ortho to each other (**1**, **4**, and **7**, as well as **10** and **13**) display the highest energy optical band gaps, whereas isomers in which they are para (**3**, **6**, and **9**, as well as **12** and **15**) display the lowest. TPEBs **7–9** with perfluorinated arene acceptor rings exhibit the smallest optical

band gaps of the acyclic compounds presented here. It is notable that **9** has a λ_{max} that appears at least as red-shifted as **15**, but in the latter case the band is a shoulder and too broadened for accurate comparison. The λ_{max} cutoff for **15**, however, extends well past 550 nm. Previous studies¹ indicate an inverse relationship with ground state net dipole: the TPEBs with the lowest calculated net dipole (the para isomers) show the most red-shifted absorbance and hence smallest optical band gap, while those with the highest (the ortho isomers) are the most blue-shifted. This trend contradicts conventional theories, which predict a correlation between optical band gap energy and conjugation linearity:¹⁴ the ortho and meta isomers, which have two linear charge-transfer conduits, possess the larger optical

(14) (a) Boldi, A. M.; Anthony, J.; Gramlich, V.; Knobler, C. B.; Boudon, C.; Gisselbrecht, J. P.; Gross, M.; Diederich, F. *Helv. Chim. Acta* **1995**, *78*, 779–796. (b) Tykwinski, R. R.; Zhao, Y. *Synlett* **2002**, 1939–1953. (c) Burri, E.; Diederich, F.; Nielsen, M. B. *Helv. Chim. Acta* **2001**, *84*, 2169–2182. (d) Wong, K. F.; Bagchi, B.; Rossky, P. J. *J. Phys. Chem. A* **2004**, *108*, 5752–5763. (e) Wei, Z. C.; Fan, H. H.; Li, N.; Wang, H. Z.; Zhong, Z. P. *J. Mol. Struct.* **2005**, *748*, 1–4.

TABLE 3. Electronic Absorption and Emission Data for TPEBs 1–15 in CH₂Cl₂

compd	lowest energy abs λ_{max} [nm] (ϵ [M ⁻¹ cm ⁻¹])	Em λ_{max} [nm]	Stokes shift	Φ_{F}^a
1	407 ^b (49 560)	544	137	0.44
2	427 (61 120)	541	114	0.38
3	438 (30 380)	546	108	0.50
4	410 ^b (60 380)	556	146	0.31
5	433 (25 460)	552	119	0.34
6	456 (38 510)	561	105	0.25
7	423 (55 690)	556	133	0.17
8	438 (40 090)	555	117	0.30
9	462 (36 100)	563	101	0.14
10	416 ^b (45 700)	563	147	0.26
11	435 (31 640)	557	122	0.35
12	454 (39 250)	563	109	0.25
13	417 (45 200)	563	146	<0.01
14	426 (50 100)	552	126	<0.01
15	448 ^b (15 690)	557	109	<0.01

^a Calculated relative to fluorescein at pH 8. ^b Approximate value as band is only a shoulder.

band gaps, while the para isomers have charge-transfer pathways with bent geometries but the smallest optical band gaps. These results parallel the findings of Diederich et al.,¹⁵ who discovered similar contradictions in the case of donor-substituted cyanoethynylethenes, and warned of the limitations of UV/vis spectrophotometry as a measure of conjugation. Meier et al. described similar effects with elongated phenyl–acetylene chromophores.¹⁶ In both cases, the usefulness of UV/vis data is relegated to probing only the change in charge transfer on going from the ground state to the excited state, and not as a measure of conjugation, for which other methods including ground state geometry and energy calculations are more appropriate.

Even with these limitations, it is likely that TPEBs **1–9** participate in a good degree of intramolecular charge transfer. The benzonitrile accepting group is weak relative to the nitrophenyl group,¹⁶ yet produces optical band gaps in the same general range and extinction coefficient (compare parts d and e of Figure 3 and cf. Table 3). Equally impressive are the benzotrifluoride acceptor systems **1–6**, with optical band gaps averaging only a few nanometers more blue-shifted. Since there are no stable resonance forms for the charge-separated excited state (which may in fact be distinct from a neutral excited state¹⁷) that place a formal negative charge on a single acceptor atom, electron withdrawal occurs principally via induction through the σ -framework. This would intuitively imply a larger optical band gap, and hence a dramatic hypsochromic shift in the absorbance spectra. From Figure 3a–c, however, this is not entirely the case: TPEBs **1–9** display the same charge-transfer properties as the resonance acceptors with bands in the same region of the UV/vis spectrum. The intensities of the longest wavelength bands are comparatively high ($\epsilon = 50000\text{--}60000$ M⁻¹ cm⁻¹) for **1**, **2**, **4**, and **7**, all of which have linear charge-transfer pathways. Taken together, these data provide further illustration of the potential limitations of electronic absorption

spectra in evaluating the complex interrelationships between optical band gap, conjugation, and charge transfer.

Comparison of **1–3** to **4–6** reveals the cumulative effect of the number of acceptor groups. TPEBs **1–3** possess one –CF₃ group per acceptor arene para to the acetylene bridge, while **4–6** possess two –CF₃ groups at the meta positions. Increasing the number of acceptor groups results in a 3–24 nm bathochromic shift in the absorption spectrum, depending on substitution isomer and solvent. Shifts are most dramatic in the para isomer **6** and least in the ortho isomer **4**. The inductive nature of the electron acceptors should negate any effect of the relative positions of the –CF₃ groups on the acceptor arene, allowing observation of the effect of changing only the number of acceptor units. Furthermore, use of symmetric acceptor units should eliminate any skewing effect of dissimilar net dipoles on the absorption and emission data. A reasonable inference from the data therefore is that “acceptor density” can be used to provide further fine-tuning of the net acceptor strength and hence the optoelectronic properties.

Absorption spectra of DBAs **16–21** are shown in Figure 4 and the data are given in Table 4. There is a 27–67 nm (depending on isomer) bathochromic shift in the lowest energy band upon planarization compared to **1–3**, reflecting the enhanced conjugation effects from increased π -orbital overlap.¹ The bis[15]DBAs **19–21** are red-shifted by 5–24 nm relative to bis[14]DBAs **16–18**. A side-by-side comparison of the spectra of TPEBs, bis[14]DBAs, and bis[15]DBAs is exemplified in Figure 5. The lowest energy bands in **16–21** are at somewhat shorter wavelengths than **22–26** due to the weaker inductive acceptors. It is noteworthy that the ortho to meta to para isomer trend in band wavelength holds for **16–18**, but not for **19–21**: **19** is slightly red-shifted from **20**. Also of note is the relative sharpness of these bands compared to the corresponding broad bands in **16–18**, which may represent increased vibronic fine structure from the rigidified molecular geometry as well as the cross-conjugated pathway. BisDBAs **19–21** also possess somewhat higher molar extinction coefficients than **16–18**. This effect was also observed in **22–26**, and is likely due to the greater linearity of the phenyl–acetylene pathways in [15]DBAs compared to [14]DBAs, which have been shown by computation and X-ray crystallography to possess greater distortion of the sp-carbon bond angles.^{1b} Also as in **22–26**, the meta isomers show the most intense charge-transfer band, and the para isomers the least. It is uncertain why this is the case, but as with the TPEBs, the para isomers represent quadrupolar chromophores, which may experience significant solvent stabilization of the excited state similar to a highly dipolar chromophore, e.g., the ortho isomers.¹⁵

Electronic Emission Spectra. The electronic emission spectra of TPEBs **1–12** in CH₂Cl₂ and benzene are shown in Figure 6 and the data are given in Tables 3 and 5. All compounds display strong fluorescence solvatochromism, experiencing bathochromic shifts of 29–55 nm in switching to the more polar solvent. In each case, the ortho isomers experience the greatest solvatochromism, and the para isomers the least. We do not suspect that the effect is due to formation of dimers or higher aggregates in solution: experiments reveal no observable concentration dependence of ¹H NMR shifts or emission wavelength over a 100-fold concentration gradient (e.g., 0.13–13 mM). This parallels our previously published data concerning the nitrophenyl analogues **13–15**: significant aggregation requires enforced planarization to the corresponding

(15) Moonen, N. N. P.; Diederich, F. *Org. Biomol. Chem.* **2004**, *2*, 2263–2266.

(16) Meier, H.; Mühling, B.; Kolshorn, H. *Eur. J. Org. Chem.* **2004**, 1033–1042.

(17) (a) Thompson, A. L.; Ahn, T.-S.; Thomas, K. R. J.; Thayumanavan, S.; Martinez, T. J.; Bardeen, C. J. *J. Am. Chem. Soc.* **2005**, *127*, 16348–16349. (b) Lee, S.; Thomas, K. R. J.; Thayumanavan, S.; Bardeen, C. J. *J. Phys. Chem. A* **2005**, *109*, 9767–9774.

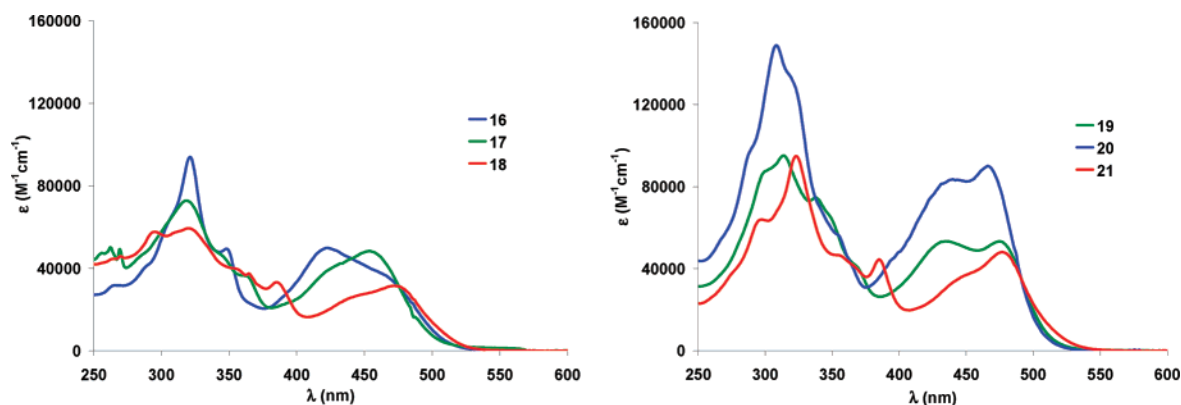


FIGURE 4. Electronic absorption spectra of (a) 16–18 and (b) 19–21. All spectra recorded in CH₂Cl₂ at analyte concentrations of 10–20 μM.

TABLE 4. Electronic Absorption and Emission Data for BisDBAs 16–21 in CH₂Cl₂

compd	lowest energy abs λ _{max} [nm] (ε [M ⁻¹ cm ⁻¹])	Em λ _{max} [nm]	Stokes shift	Φ _F ^a
16	450 ^b (41 430)	554	104	0.35
17	454 (48 310)	544	90	0.46
18	472 (31 480)	555	83	0.33
19	474 (53 300)	550	76	0.23
20	466 (90 020)	551	85	0.15
21	477 (48 080)	558	81	0.25

^a Calculated relative to fluorescein at pH 8. ^b Approximate value as band is only a shoulder.

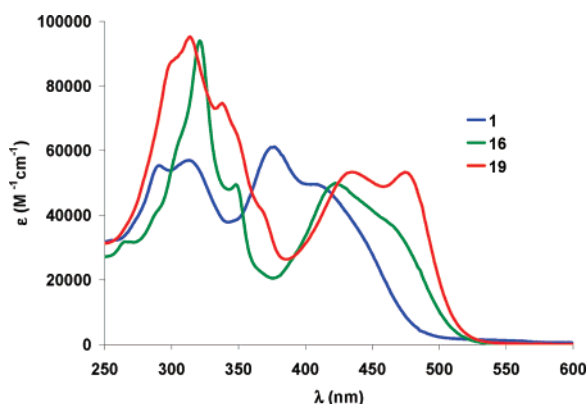


FIGURE 5. Electronic absorption spectra of TPEB 1, bis[14]DBA 16, and bis[15]DBA 19.

bis(dehydrobenzoannuleno)benzenes (vide infra).^{1b} Variation in substitution isomer has little effect on emission wavelength in CH₂Cl₂, although the trend of meta < ortho < para, in order of increasing wavelength, holds for all compounds. In benzene the order is ortho < meta < para. Since this positive solvatochromism results from solvent stabilization of the charge-transfer excited state,^{18a–g} we are led to the intuitive inference that the ortho isomers experience the greatest stabilization in the excited

(18) (a) Seo, J.; Kim, S.; Park, S. Y. *J. Am. Chem. Soc.* **2004**, *126*, 11154–11155. (b) Yam, V. W.-W.; Wong, K. M.-C.; Zhu, N. *J. Am. Chem. Soc.* **2002**, *124*, 6506–6507. (c) Hong, J. W.; Woo, H. Y.; Liu, B.; Bazan, G. C. *J. Am. Chem. Soc.* **2005**, *127*, 7435–7443. (d) Spange, S.; Prause, S.; Vilsmeier, E.; Thiel, W. R. *J. Phys. Chem.* **2005**, *109*, 7280–7289. (e) Gawinecki, R.; Trzebiatowska, K. *Pol. J. Chem.* **2001**, *75*, 231–239. (f) Anstead, G. M.; Katzenellenbogen, J. A. *J. Phys. Chem.* **1988**, *92*, 6249–6258. (g) Lackowicz, J. R. *Principles of Fluorescence Spectroscopy*; Plenum: New York, 1983. (h) Drushel, H. V.; Sommers, A. L.; Cox, R. C. *Anal. Chem.* **1963**, *35*, 2166–2172.

state by the more polar solvent and possess the greatest net dipole in the ground state. The Stokes shift trends in CH₂Cl₂ support this hypothesis: higher dipole moments lead to greater excited state stabilization by polar solvents, resulting in higher Stokes shifts.^{18f,g} Emission wavelengths are more spread out in benzene, perhaps more accurately reflecting the variations in electronic states with substitution isomer.

The emission spectra of 1–6 in CH₂Cl₂ expanded in the 520–600 nm region are shown in Figure 7 and illustrate the overall effect of both isomer and number of acceptor groups. The most red-shifted of the benzotrifluoride TPEBs, 3, is 6 nm behind 5, the most blue-shifted of the bis(trifluoromethyl)phenyl compounds, showing that choice of acceptor strength is more effective at tuning fluorescence than choice of substitution isomer. TPEB 6 is conspicuously red-shifted relative to 1–5, emitting at nearly the same wavelength as 10 and 12, both of which are resonance acceptors. Note as well in Table 3 the similarity in extinction coefficient, showing that the strongly inductive acceptor group displays optical band gaps (and potential nonlinear optical susceptibilities) comparable to that of the relatively weak resonance acceptors. These similarities extend also to 13–15, which have been shown to possess attractive NLO characteristics.⁶

The electronic emission spectra of 16–21 in CH₂Cl₂ and benzene are shown in Figure 8 and the data are tabulated in Tables 4 and 5. The bisDBAs exhibit the same dramatic solvatochromism as the TPEBs (see the Supporting Information, Figure S1, for additional representative spectra). Planarization has much less effect on the emission than the absorption, however. Maxima rarely differ from 1–3 in either solvent by more than 12 nm, and never by more than 20 nm. This may imply that planarization has less of an effect on the lowest vibrational level of the first excited state than the ground state. Consequently, Stokes shifts are smaller for all isomers. In benzene, the para isomers are again conspicuously red-shifted relative to the ortho and meta isomers. In the cases of the DBAs the wavelength order in both solvents is meta < ortho < para. This may indicate an enhanced dipole in the ortho DBAs upon planarization from 1. The bisDBAs presented here are significantly (60–80 nm) blue-shifted relative to 22–26, which emit in toluene in the orange-red region (all emission of 22–26 is quenched in CH₂Cl₂).^{1b} This large difference is likely due to a much lower lying excited state in the strong resonance acceptor systems. Segment-localized FMOs explain this effect: when the HOMO is localized on the donor segment and the LUMO is localized on the acceptor segment, changes in the strength or

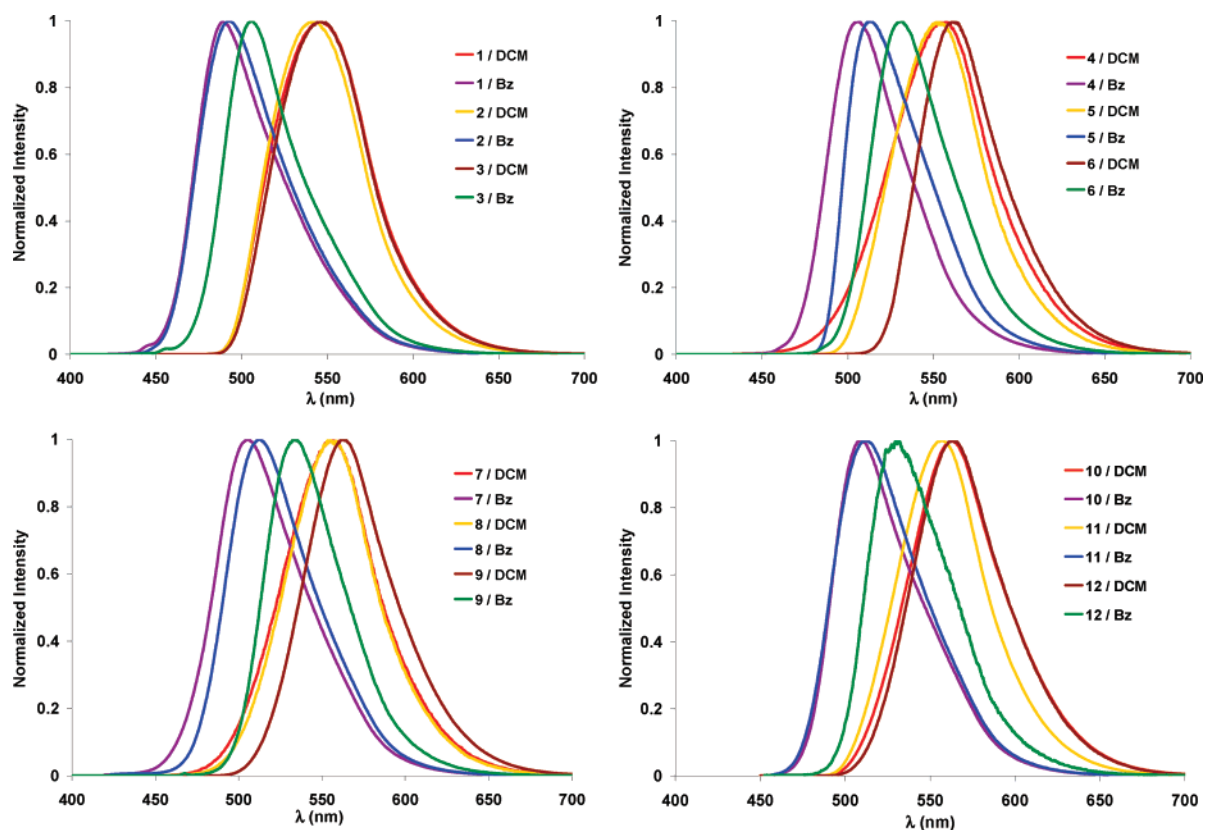


FIGURE 6. Electronic emission spectra of (a) 1–3, (b) 4–6, (c) 7–9, and (d) 10–12 in CH_2Cl_2 (DCM) and benzene (Bz). All spectra were recorded at analyte concentrations of 15–25 μM with excitation at 450 nm.

TABLE 5. Electronic Emission Data for 1–12 and 16–21 in Benzene

compd	Em λ_{max} (nm) ^a	compd	Em λ_{max} (nm) ^a
1	490	10	508
2	493	11	512
3	506	12	530
4	506	16	504
5	514	17	501
6	531	18	521
7	505	19	503
8	512	20	499
9	534	21	522

^a Excitation at 450 nm.

type of either group can affect each MO nearly independently.^{1c,7} Here, we retain the strong donor group and switch to a weaker acceptor group. Accordingly, a greater effect is seen in the emission spectra than the absorption spectra.

The fluorescence quantum yields of 1–12 and 16–21 in CH_2Cl_2 were calculated from the steady-state spectroscopic measurements by using the techniques described by Drushel et al.^{18h} The values are given in Tables 3 and 4, and the quantum yields are also shown graphically in Figure 9 (13–15 and 22–26 are calculated to have quantum yields of <0.01).^{1b} The general trend follows the concept of decreasing quantum yield with increasing acceptor strength: as optical band gaps narrow, nonradiative de-excitation via dissipative/vibronic coupling becomes more accessible.^{1b,c,19} In most cases presented here, the meta isomers show the highest Φ_f , possibly for the same reasons they exhibit higher charge-transfer band intensities in the absorption spectra. Notable exceptions are 2 and 20, although it is unclear why

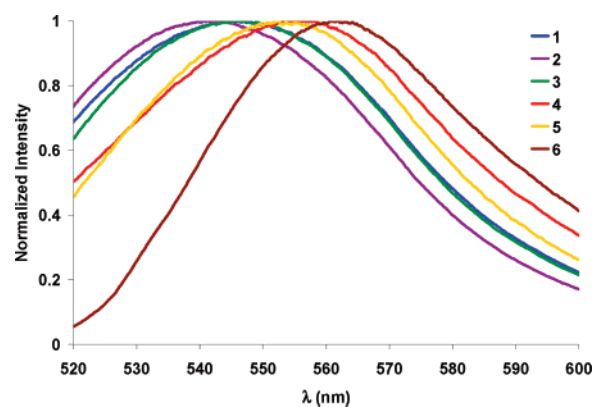


FIGURE 7. Expanded electronic emission spectra of 1–6 in CH_2Cl_2 .

these are the case. As noted above, however, conjugation pathways in 19–21 are structurally more similar to those in 1–3 than are 16–18, so the cause for the deviation may be the same in both systems. From these data, 7–9 appear to exhibit qualitative acceptor strength equal to or greater than even the benzonitrile analogues. If the absorption spectrum can be taken as a quantitative measure of excitation optical band gaps, then we have in 1–9, and especially in 3, TPEBs that exhibit relatively narrow optical band gaps and high quantum yields. Thus, it is demonstrated once again that the correct choice of acceptor identity can optimize various desired optical properties

(19) (a) Tolbert, L. M.; Nesselroth, S. M.; Netzel, T. L.; Raya, N.; Stapleton, M. *J. Phys. Chem.* **1992**, *96*, 4492–4496. (b) Engelman, R.; Jortner, *J. Mol. Phys.* **1970**, *18*, 145–154. (c) Caspar, J. V.; Meyer, T. J. *J. Phys. Chem.* **1983**, *87*, 952–957.

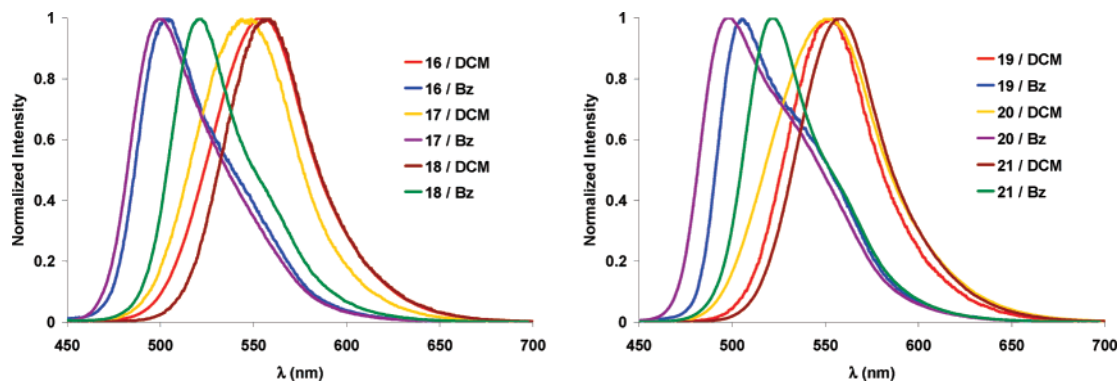


FIGURE 8. Electronic emission spectra of (a) 16–19 and (b) 19–21 in CH_2Cl_2 (DCM) and benzene (Bz). All spectra were recorded at analyte concentrations of 15–25 μM with excitation at 450 nm.

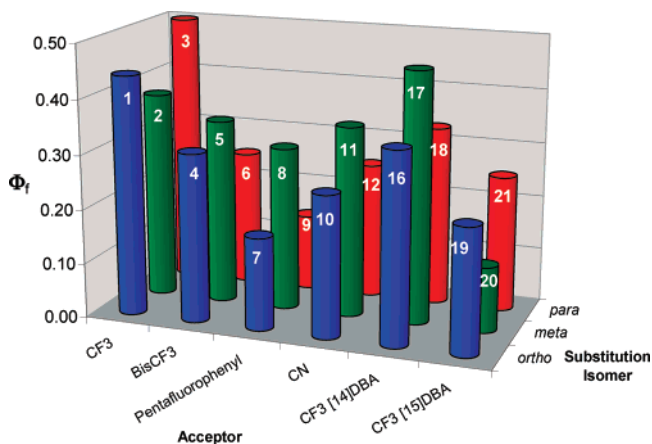


FIGURE 9. Quantum yield trends for TPEBs 1–12 and bisDBAs 16–21 in CH_2Cl_2 .

for specialized applications. The bis[14]DBAs exhibit quantum yields comparable to 1–3, while the bis[15]DBAs are consistently lower. This was also observed for the all-donor analogues,^{1b} and may indicate increased $\pi-\pi^*$ -like character of the $S_0 \rightarrow S_1$ transition for 16–21 relative to 22–26. Quantum yields in benzene have been calculated for many of the TPEB compounds,^{1d} and are generally higher than in dichloromethane due to decreased solvent and dipole interaction with lower internal and external conversion rate constants.

Film Spectra. Because of the potential for these systems to serve as components of organic optical devices, as well as the striking emission solvent sensitivity, we determined the absorption and emission profiles of thin films to examine how the solid state properties compared to those in solution. Compounds 1–9 were drop-cast from CH_2Cl_2 solution onto cleaned glass microscope cover slides and the resulting films were placed under vacuum for 1 h to remove residual solvent. The resulting absorption and emission spectra are shown in Figure 10 and the relevant maxima are listed in Table 6. The features of the absorption spectra are considerably broadened compared to the solution-phase spectra, but in general the absorption profiles retain their characteristic band shapes. The lowest energy λ_{max} for most compounds remains remarkably similar to that in CH_2Cl_2 , typically with shifts of less than 12 nm. For 1–3 and 7–9, the λ_{max} are either equal to or lower than those in CH_2Cl_2 , possibly reflecting less interaction between the molecules and the substrate, resulting in slightly larger optical band gaps. TPEB 4 shows a charge transfer band potentially red-shifted by a few

nanometers, but as in all ortho isomers, the band overlaps with the next highest band, making the exact determination of the λ_{max} difficult. TPEB 5, however, displays an 18 nm red-shift relative to CH_2Cl_2 . TPEB 6 exhibits a band ca. 10 nm blue-shifted from CH_2Cl_2 , but also shows an additional anomalous band at 495 nm. Additional solid-state samples of 6 also showed this band. While not an artifact, we are currently at a loss to explain the origin of this new peak. Overall, the lack of significant red shifting from fluoroaryl/electron-rich aryl interaction is notable. A combination of rigidity enforced by the alkynes and steric congestion of partially perfluorinated, ortho-fused arylacetylenes may serve to inhibit the orientation of the ring systems into arrangements optimal for $\pi-\pi$ interaction.

The emission spectra of the thin films consistently display maxima between 5 and 16 nm blue-shifted from those in CH_2Cl_2 , with the exception of 7, with an emission λ_{max} almost halfway between CH_2Cl_2 and benzene and an additional shoulder around 487 nm, and 9, which is significantly blue-shifted from benzene. As a group, the perfluoroarene acceptor compounds 7–9 exhibit the most consistent blue-shifting relative to solvent spectra, implying the least amount of surface interaction of the systems examined here.

Self-Association. As stated above, aggregation of the TPEB skeleton in solution requires enforced planarization to the corresponding bis(dehydrobenzoannuleno)benzenes. In prior studies, bisDBAs 22–26 were observed to exhibit significant aggregation due to π -stacking and dipole–dipole attraction between donor and acceptor rings, which resulted in dramatic (over 1 ppm) upfield shifts of ^1H NMR signals with increasing concentration and association constants of up to $K_2 = 5000 \text{ M}^{-1}$.^{1b} In the case of 26, the molecule rapidly decomposed in deacidified CDCl_3 , possibly due to topochemical diacetylene polymerization induced by the strong association.²⁰ Similar experiments show that 16–21 do not display such extreme behavior, exhibiting only relatively small (0.005–0.249 ppm, average 0.06 ppm) proton shifts over a several 100-fold concentration gradient (0.27–9.9 mM). We calculated the association constants for the protons of DBA 19 as the most dramatic example (Figure 11, see the Supporting Information, Figure S2, for additional representative plots for 16 and 18),²¹ assuming that the monomer–dimer equilibrium was the predominant process as was the case in 22–26. The small values

(20) Baldwin, K. P.; Matzger, A. J.; Scheiman, D. A.; Tessier, C. A.; Vollhardt, K. P. C.; Youngs, W. J. *Synlett* **1995**, 1215–1218.

(21) Bangerter, B. W.; Chan, S. I. *J. Am. Chem. Soc.* **1969**, *91*, 3910–3921.

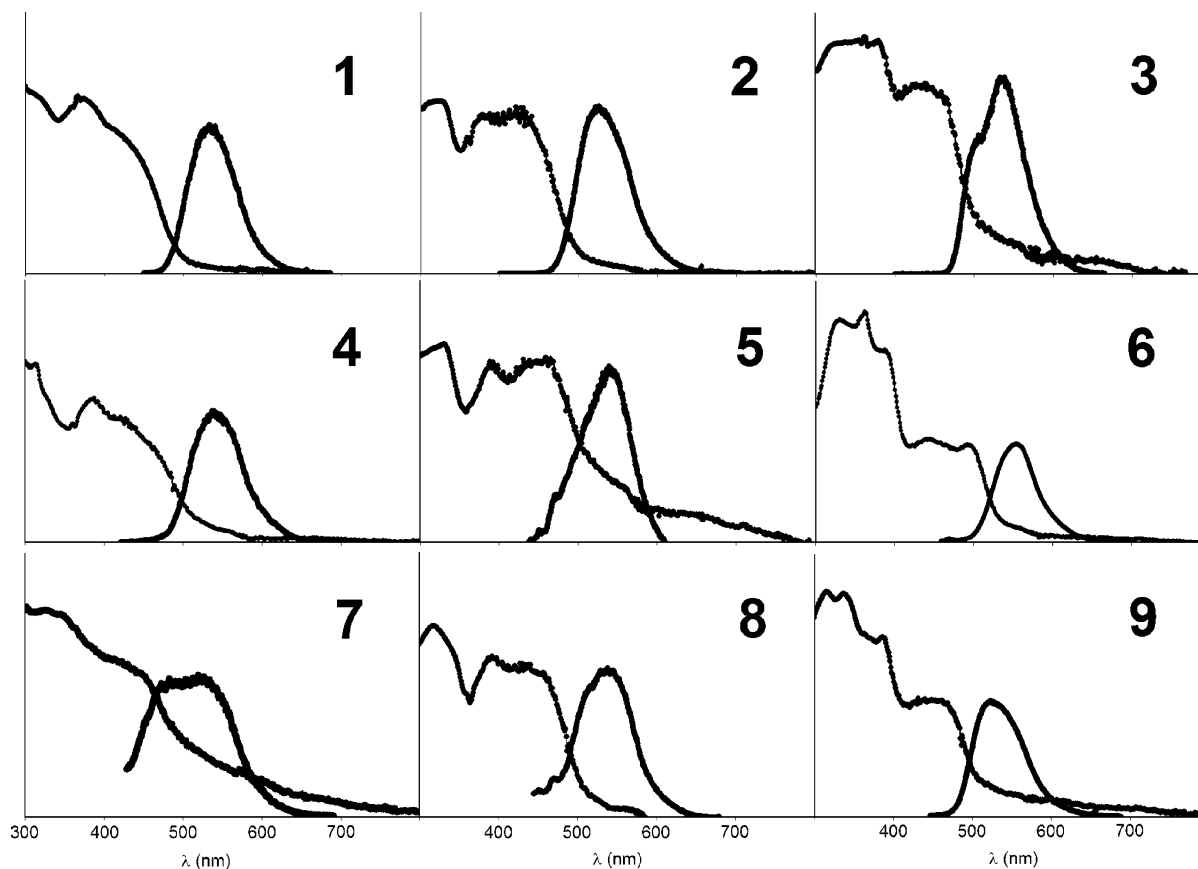


FIGURE 10. Absorption (left) and normalized (right) emission spectra of drop-cast films of 1–9.

TABLE 6. Electronic Absorption and Emission Data for Films of TPEBs 1–9

compd	lowest energy abs (nm)	Em λ_{\max} (nm)	Stokes shift
1	405	534	129
2	427	527	100
3	438	538	100
4	422	540	118
5	451	539	88
6	446, 495	556	110, 61
7	415	529	114
8	437	539	102
9	452	525	73

(average $K_2 = 178 \pm 41 \text{ M}^{-1}$) likely reflect both a much smaller degree of intermolecular attraction as well as a much greater solvent interaction relative to 22–26. Unlike 26, 16–21 are completely stable when left in CDCl_3 solution for several days. It is likely that the weaker acceptor groups cannot induce the degree of aggregation necessary for decomposition/polymerization. This greater stability implies better processability for materials based on inductive $-\text{CF}_3$ acceptors versus strong resonance acceptors, although a larger optical band gap is achieved.

Conclusions

Two-dimensional donor/acceptor tetrakis(phenylethynyl)benzenes 1–9 and bis(dehydrobenzoannuleno)benzenes 16–21 have been prepared. The fluorinated acceptor groups, while weaker than previously reported nitrile- or nitro-functionalized analogues 10–15 and 22–26,^{1a,b,d} lead to strongly fluorescent

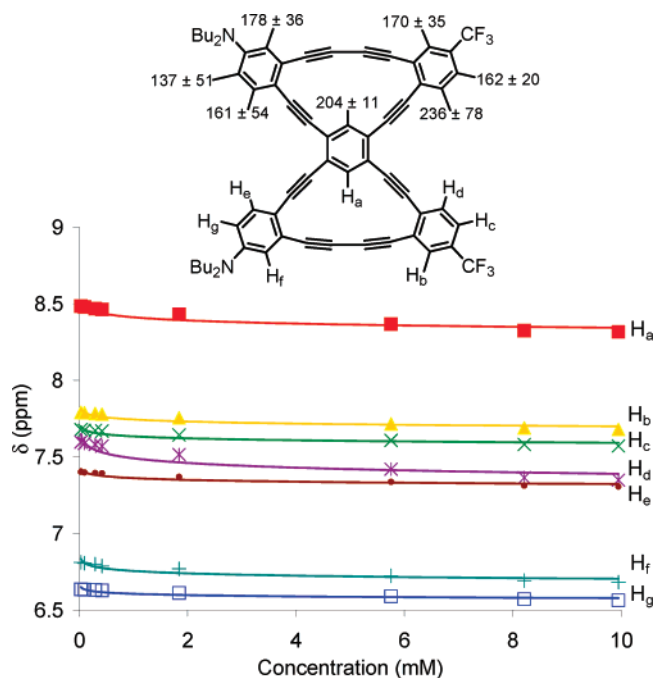


FIGURE 11. Concentration-dependent chemical shifts (bottom) and calculated association constants K_2 (top, M^{-1}) of the aromatic protons of DBA 19 in CDCl_3 at 20 °C; values were calculated using the methods described in ref 21.

intramolecular charge transfer. TPEBs 1–9 display optical band gaps very near 10–15, while retaining high fluorescence quantum yields for relatively small chromophores, providing

unique and promising candidates for nonlinear optical device materials.⁶ The inductive $-\text{CF}_3$ acceptor group is quite effective at participating in ICT behavior, despite the lack of a formal resonance pathway for full conjugation. This may imply that electronic transitions with both $\pi-\pi^*$ and formal charge transfer characteristics dominate, producing a “best of both worlds” situation that could be exploited in materials design.^{7,22,23} The bis $-\text{CF}_3$ acceptors show significant bathochromic shifts relative to a single $-\text{CF}_3$ group, demonstrating the cumulative effect of acceptor strength and “acceptor density”. The pentafluorophenyl acceptor TPEBs show the most red-shifting of absorption and emission wavelengths, and approach the benzonitrile and nitrophenyl systems in terms of optical band gap narrowing ability. In thin films, on the other hand, their spectra indicate the least amount of substrate interaction of the compounds studied herein.

BisDBAs **16–21** represent planarized versions of fluorophores **1–3**, with enhanced conjugation efficiency from greater π -orbital overlap, and accordingly smaller optical band gaps. They exhibit higher quantum yields and greater solution stability than our previously examined D/A DBAs. Additionally, the full isomer/ring size array is accessible in **16–21**, whereas the nitro analogue of **18** could not be isolated.

Our results support findings by Diederich et al.¹⁵ questioning the utility of UV/vis data alone as a measure of conjugation pathway efficiency. One possible explanation for the lower experimental optical band gaps in the systems with bent charge transfer pathways is that fundamentally different transitions dominate in the quadrupolar chromophores, causing dramatically different optical behavior than is observed in the dipolar analogues.^{6c} It may be that the HOMO–LUMO transition is in fact not the lowest energy transition for these molecules. On the other hand, Stokes shift seems well correlated to conjugation pathway linearity, with the ortho isomers displaying the highest values, and (presumably) the highest ground state net dipoles.

The effectiveness of the $-\text{CF}_3$ acceptor has led us to investigate its utility in further studies involving modification of the donor group to one containing a meta electron transport pathway. Donor/acceptor systems with such geometries have been shown to possess intriguing potential as unidirectional one-electron wires for use in solar electrochemical cells^{17,24} and provide insight into excited state behavior.^{18f,25} The results of these new studies will be reported in due course.

Experimental Section

General Methods. These are described in ref 1b.

General Alkyne Coupling Procedure A. Haloarene (1 equiv) and TMSA (1.5 equiv per transformation unless otherwise noted) were dissolved in $i\text{Pr}_2\text{NH}:\text{THF}$ (1:1, 0.05 M) and the solution

purged for 30 min with bubbling Ar. $\text{Pd}(\text{PPh}_3)_4$ (0.03 equiv per transformation) and CuI (0.06 equiv per transformation) were added and the solution was purged another 20 min. The reaction mixture was stirred at 65 °C for 12–48 h under an Ar atmosphere. Upon completion, the mixture was concentrated and filtered through a pad of silica gel eluting with hexanes. The solvent was removed in vacuo and the crude material was used without further purification.

General Alkyne Coupling Procedure B. Acceptor haloarene (3 equiv per transformation unless otherwise noted) and KOH (aq, 50 wt %, 10 equiv) were dissolved in $i\text{Pr}_2\text{NH}:\text{THF}$ (1:1, 0.03 M) and the solution was purged for 30 min with bubbling Ar. $\text{Pd}(\text{PPh}_3)_4$ (0.03 equiv per transformation) and CuI (0.06 equiv per transformation) were added and the solution was purged another 20 min. Trimethylsilyl-protected diyne (1 equiv) was purged in THF solution for 50 min with bubbling Ar, and then injected via syringe pump into the stirred haloarene solution over 12 h at 65 °C under an Ar atmosphere. The reaction mixture was stirred an additional 12–48 h until complete by TLC. The mixture was then concentrated, rediluted with CH_2Cl_2 , and filtered through a pad of silica gel. The solvent was removed in vacuo and the crude material was purified by column chromatography.

General Alkyne Coupling Procedure C. Acceptor segment **31** (2.3 equiv) and the appropriate isomer of dibromodiodobenzene (1 equiv) were dissolved in $i\text{Pr}_2\text{NH}:\text{THF}:\text{MeOH}$ (3:3:1, 0.003 M) and the solution was purged for 30 min with bubbling Ar. $\text{PdCl}_2(\text{PPh}_3)_2$ (0.03 equiv per transformation), CuI (0.06 equiv per transformation), and K_2CO_3 (8 equiv per transformation) were added and the solution was purged another 20 min. The reaction mixture was stirred at room temperature for 24–48 h under an Ar atmosphere until complete by TLC. The mixture was then concentrated, rediluted with hexanes, and filtered through a pad of silica gel. The solvent was removed in vacuo and the crude material was used without further purification.

General Alkyne Coupling Procedure D. Acceptor-functionalized tetrayne, $\text{PdCl}_2(\text{PPh}_3)_2$ (0.03 equiv per transformation), and CuI (0.06 equiv per transformation) were dissolved in $i\text{Pr}_2\text{NH}:\text{THF}$ (1:1, 0.008 M) and the solution was purged for 30 min under bubbling Ar. Diyne **33**^{1b} (2.3 equiv) was dissolved in THF (0.04 M), the solution was purged for 30 min under bubbling Ar, and then injected via syringe pump into the stirred polyene solution over 8 h at 55 °C under an Ar atmosphere. The reaction was stirred an additional 12–24 h until complete by TLC. The mixture was then concentrated, rediluted with hexanes: CH_2Cl_2 (4:1), and filtered through a pad of silica gel. The solvent was removed in vacuo, and the crude material was purified by column chromatography.

General Pd-Catalyzed Cyclization Procedure E. Annulene precycle was dissolved in THF, Et_2O , and MeOH (2:1:0.01, 0.005 M) and Bu_4NF (TBAF, 1.0 M soln in THF, 10 equiv) was added. The solution was stirred at room temperature until complete by TLC (typically <1 h). The reaction mixture was then concentrated, dissolved in Et_2O , and washed with H_2O (3×50 mL). The organic phase was collected, dried over MgSO_4 , and filtered through a pad of silica gel eluting with hexanes. The solvent was removed in vacuo and deprotected precycle was dissolved in THF (0.005 M). $\text{PdCl}_2(\text{dppe})$ (0.1 equiv per transformation), CuI (0.2 equiv per transformation), and I_2 (0.25 equiv per transformation) were dissolved in $i\text{Pr}_2\text{NH}:\text{THF}$ (1.4:1, ~ 0.5 L per mmol precycle). To this mixture was injected the deprotected precycle solution via syringe pump over 40 h at 60 °C. The reaction mixture was stirred until complete by TLC, then concentrated, rediluted in hexanes: CH_2Cl_2 (4:1), and filtered through a pad of silica gel. The solvent was removed in vacuo and the product was triturated with hexanes.

General Cu-Mediated Cyclization Procedure F. Annulene precycle was dissolved in THF, Et_2O , and MeOH (2:1:0.01, 0.005

(22) For example: (a) Vaganova, E.; Yitzchaik, S.; Shapiro, L.; Sigalov, M.; Khodorkovsky, V. *Adv. Mater.* **2006**, *12*, 1669–1671. (b) Yeh, S.-J.; Chen, H.-Y.; Wu, M.-F.; Chan, L.-H.; Chiang, C.-L.; Chen, C.-T.; Lee, J.-H. *Org. Electron.* **2006**, *7*, 137–143 and references cited therein.

(23) (a) Sheats, J. R. *J. Mater. Res.* **2004**, *19*, 1974–1989. (b) Dhananabalan, A.; Dos Santos, D. S., Jr.; Mendonca, C. R.; Misoguti, L.; Balogh, D. T.; Giacometti, G. A.; Zillio, S. C.; Oliveira, O. N., Jr. *Langmuir* **1999**, *15*, 4560–4564. (c) Michl, J. In *Photochromism—Molecules and Systems*; Durr, H., Bouas-Laurent, H., Eds. Elsevier: Amsterdam, The Netherlands, 1990; pp 919–930.

(24) (a) Gaab, K. M.; Thompson, A. L.; Xu, J.; Martinez, T. J.; Bardeen, C. J. *J. Am. Chem. Soc.* **2003**, *125*, 9288–9289. (b) Thompson, A. L.; Gaab, K. M.; Xu, J.; Bardeen, C. L.; Martinez, T. J. *J. Phys. Chem. A* **2004**, *108*, 671–682.

(25) (a) Roberts, J. C.; Pincock, J. A. *J. Org. Chem.* **2006**, *71*, 1480–1492. (b) Zimmerman, H. E. *J. Am. Chem. Soc.* **1995**, *117*, 8988–8991. (c) Lewis, F. D.; Yang, J.-S. *J. Am. Chem. Soc.* **1997**, *119*, 3834–3835. (d) Yamaguchi, Y.; Kobayashi, S.; Wakamiya, T.; Matsubara, Y.; Yoshida, Z. *Angew. Chem., Int. Ed.* **2005**, *44*, 7040–7044.

M) and TBAF (1.0 M soln in THF, 10 equiv) was added. The solution was stirred at room temperature until it was determined to be complete by TLC (typically <1 h). The reaction mixture was then concentrated, dissolved in Et₂O, and washed with H₂O (3 × 50 mL). The organic phase was collected, dried with MgSO₄, and filtered through a pad of silica gel eluting with hexanes. The solvent was removed in vacuo and deprotected precycle was dissolved in pyridine (0.005 M). Cu(OAc)₂ (12.5 equiv per transformation) and CuCl (10 equiv per transformation) were dissolved in pyridine: MeOH (1.5:1, ~2.5 L per mmol precycle). To this mixture was injected the deprotected precycle solution via syringe pump over 40 h at 60 °C. The reaction mixture was stirred until complete by TLC, then concentrated, rediluted in hexanes:CH₂Cl₂ (4:1), and filtered through a pad of silica gel. The solvent was removed in vacuo and the product was triturated with hexanes.

1,4-Bis[(4'-N,N-dibutylaminophenyl)ethynyl]-2,5-bis[(4'-trifluoromethylphenyl)ethynyl]benzene (3). TMSA (130 mg, 1.3 mmol) was coupled to diyne **16**^{1c} (304 mg, 0.44 mmol) by using general procedure A. The resulting red oil was coupled to 4-bromobenzotrifluoride (990 mg, 4.4 mmol) by using general procedure B. The crude material was chromatographed on silica gel (4:1 hexanes:CH₂Cl₂) to yield **3** (255 mg, 67%) as a bright yellow solid. Mp 125–127 °C dec. ¹H NMR (CDCl₃) δ 7.71 (s, 2H), 7.60–7.70 (m, 8H), 7.40 (d, *J* = 8.4 Hz, 4H), 6.60 (d, *J* = 8.4 Hz, 4H), 3.32 (t, *J* = 7.5 Hz, 8H), 1.61 (quin, *J* = 6.6 Hz, 8H), 1.39 (sext, *J* = 7.2 Hz, 8H), 1.00 (t, *J* = 7.2 Hz, 12H). ¹³C NMR (CDCl₃) δ 148.6, 134.8, 133.4, 132.2, 127.4, 125.9, 125.6, 125.5, 124.6, 111.5, 108.4, 98.0, 93.6, 90.8, 86.0, 51.0, 29.7, 20.6, 14.3. IR (NaCl) ν 2197, 1602, 1519, cm⁻¹. HRMS (ESI) for C₅₆H₅₄F₆N₂ [M + H]⁺ calcd 869.4264, found 869.4268. MS (APCI) *m/z* ([isotope], %) 871.3 (M⁺[²¹³C], 18), 870.5 (M⁺[¹³C], 62), 869.2 (M⁺, 100). UV (CH₂Cl₂) λ_{max} (log ε) 383 (4.64), 440 (4.48). Em λ_{max} 546.

1,4-Bis[(4'-N,N-dibutylaminophenyl)ethynyl]-2,5-bis[(2',3',4',5',6'-pentafluorophenylethynyl)benzene (9). TMSA (94 mg, 0.96 mmol) was coupled to diyne **16**^{1c} (221 mg, 0.32 mmol) by using general procedure A. The resulting red oil was desilylated by dissolving in THF:MeOH (5:1, 40 mL) with KOH (90 mg, 1.6 mmol) and stirring for 2 h. The red solution was concentrated in vacuo and filtered through a pad of silica with CH₂Cl₂. After reconcentration, the red oil was immediately coupled to pentafluoriodobenzene (470 mg, 1.60 mmol) by using general procedure B with omission of KOH in the reaction mixture and injection of the deprotected alkyne over 18 h at 45 °C. The crude material was chromatographed on silica gel (5:1 hexanes:CH₂Cl₂) to yield **9** (100 mg, 35%) as a bright yellow solid. Mp 130–170 °C dec. ¹H NMR (CDCl₃) δ 7.72 (s, 2H), 7.38 (d, *J* = 9.0 Hz, 4H), 6.58 (d, *J* = 9.0 Hz, 4H), 3.30 (t, *J* = 7.5 Hz, 8H), 1.59 (quin, *J* = 8.1 Hz, 8H), 1.38 (sext, *J* = 7.5 Hz, 8H), 0.97 (t, *J* = 7.5 Hz, 12H). ¹³C NMR (CDCl₃) δ 149.5, 148.5, 146.9, 139.5, 135.5, 133.5, 125.5, 123.8, 111.2, 111.2, 108.3, 100.2, 98.6, 85.4, 78.4, 50.9, 29.6, 20.6, 14.2. IR (NaCl): ν 3014, 2281, 2187, 1728, 1689, 1575, 1571, 1524 cm⁻¹. HRMS (ESI) for C₅₄H₄₆F₁₀N₂ [M + H]⁺ calcd 913.3574, found 913.3576. MS (APCI) *m/z* ([isotope], %) 915.5 (M⁺[²¹³C], 16), 914.5 (M⁺[¹³C], 50), 913.2 (M⁺, 100). UV (CH₂Cl₂) λ_{max} (log ε) 385 (4.74), 462 (4.56). Em λ_{max} 563.

Acceptor Triazene 29. Aniline **28** (6.71 g, 23 mmol) and CH₃CN (5 mL) were cooled in an ice salt bath to -5 °C and concd HCl (21 mL) was added dropwise. A solution of NaNO₂ (3.85 g, 56 mmol) in H₂O (3 mL) was added dropwise maintaining the temperature below 0 °C. Upon completion, the reaction mixture was stirred at -5 °C for 15 min. In a separate flask, K₂CO₃ (18.3 g, 130 mmol) and piperidine (21.5 g, 302 mmol) were dissolved in CH₃CN (110 mL) and H₂O (300 mL) and cooled to 0 °C in an ice salt bath. The reaction mixture was transferred into the basic solution via canula while maintaining temperature below 5 °C, and then left stirring open to air for 12 h while warming to rt. The mixture was then concentrated and taken up in Et₂O, then washed successively with H₂O, brine solution, and H₂O (100 mL each).

The organic phase was dried over MgSO₄ and filtered through a pad of silica gel eluting with hexanes:CH₂Cl₂ (7:3). The solvent was removed in vacuo to yield **29** (7.4 g, 83%) as an orange oil. ¹H NMR (CDCl₃) δ 8.08 (s, 1H), 7.52 (d, 1H, *J* = 5.1 Hz), 7.45 (d, 1H, *J* = 5.1 Hz), 3.97 (s, 2H), 3.84 (s, 2H), 1.75 (m, 6H). ¹³C NMR (CDCl₃) δ 153.0, 136.4, 136.3, 126.0, 125.9, 117.4, 96.0, 53.4, 44.6, 26.7, 24.4. IR (NaCl) ν 2938, 2853, 1600, 1423, 1388, 1320, 1253, 1164, 1118, 1075 cm⁻¹. HRMS (EI) for C₁₂H₁₃F₃IN₃ [M]⁺ calcd 383.0106, found 383.0100. MS (APCI) *m/z* ([isotope], %) 383.0 (M⁺, 100), 384.0 (M⁺ [¹³C], 9).

Acceptor Iodide 30. Triazene **29** (7.3 g, 19 mmol), PdCl₂(PPh₃)₂ (134 mg, 0.19 mmol), and CuI (0.073 g, 0.38 mmol) were dissolved in THF (75 mL) and *i*-Pr₂NH (75 mL), and the solution was purged with bubbling Ar for 30 min. TIPSA (6.4 mL, 29 mmol) was injected via syringe, and the reaction mixture was left stirring 24 h at room temperature under an atmosphere of Ar. The reaction mixture was then concentrated, rediluted in hexanes:CH₂Cl₂ (2:1), and filtered through a pad of silica gel. The solvent was removed in vacuo, and the crude material was redissolved in MeI (30 mL). The solution was stirred for 72 h at 155 °C in a high-pressure reaction vessel. The reaction mixture was then cooled, concentrated, rediluted in hexanes:CH₂Cl₂ (4:1), and filtered through a pad of silica gel. The solvent was removed in vacuo to yield **30** (6.4 g, 74%) as a red oil. ¹H NMR (CDCl₃) δ 7.96 (d, 1H, *J* = 9.0 Hz), 7.68 (d, 1H, *J* = 2.7 Hz), 7.20 (dd, 1H, *J* = 9.0, 2.7 Hz), 1.17 (s, 21H). ¹³C NMR (CDCl₃) δ 139.6, 131.3, 129.7, 125.7, 106.9, 105.4, 98.0, 90.5, 81.8, 18.9, 11.5. IR (NaCl) ν 2952, 2889, 2160, 1597, 1565, 1462, 1395, 1328, 1280, 1252, 1209, 1177, 1126, 1082 cm⁻¹. HRMS (EI) for C₁₈H₂₄F₃ISi [M]⁺ calcd 452.0644, found 452.0641. MS (APCI) *m/z* ([isotope], %) 452.4 (M⁺, 100), 453.3 (M⁺ [¹³C], 31).

Acceptor Segment 31. Iodoarene **30** (6.4 g, 14 mmol), PdCl₂(PPh₃)₂ (390 mg, 0.56 mmol), and CuI (0.11 g, 1.1 mmol) were dissolved in THF (100 mL) and *i*Pr₂NH (100 mL), and the solution was purged with bubbling Ar for 30 min. TMSA (4 mL, 28 mmol) was injected via syringe, and the reaction mixture was stirred 24 h at room temperature under an atmosphere of Ar. The reaction mixture was then concentrated, rediluted in hexanes:CH₂Cl₂ (2:1), and filtered through a pad of silica gel. The solvent was removed in vacuo to yield **31** (5.6 g, 95%) as a yellow solid. Mp 65–69 °C. ¹H NMR (CDCl₃) δ 7.69 (s, 1H), 7.57 (d, 1H, *J* = 8.1 Hz), 7.46 (d, 1H, *J* = 8.1 Hz), 1.16 (s, 21H), 0.26 (s, 9H). ¹³C NMR (CDCl₃) δ 133.5, 129.9, 129.3, 126.7, 124.5, 122.0, 104.0, 102.3, 101.5, 97.4, 81.8, 18.9, 11.6, 0.03. IR (NaCl) ν 2955, 2944, 2890, 2865, 2156, 2058, 1608, 1464, 1406, 1331, 1262, 1248, 1136, 1172 cm⁻¹. HRMS (EI) for C₂₃H₃₃F₃Si₂ [M]⁺ calcd 422.2073, found 422.2076. MS (APCI) *m/z* ([isotope], %) 422.2 (M⁺, 100), 423.3 (M⁺ [¹³C], 56).

Acceptor-Functionalized Aryl Bromide 32. Diyne **31** (200 mg, 0.54 mmol) was coupled to 1,5-dibromo-2,4-diiodobenzene (100 mg, 0.24 mmol) by using general procedure C to yield **32** (205 mg, 93%) as a yellow solid. Mp 52–53 °C. ¹H NMR (CDCl₃) δ 7.92 (s, 1H), 7.77 (s, 2H), 7.74 (s, 1H), 7.67 (d, 2H, *J* = 8.1 Hz), 7.56 (d, 2H, *J* = 8.1 Hz), 1.10 (s, 42H). ¹³C NMR (CDCl₃) δ 137.7, 136.1, 133.2, 132.9, 130.7, 129.9, 128.6, 127.0, 126.1, 124.8, 124.5, 103.7, 98.2, 92.8, 92.0, 18.9, 11.5. IR (NaCl) ν 2944, 2890, 2867, 2157, 1614, 1490, 1452, 1382, 1324, 1258, 1200, 1130, 1068 cm⁻¹. MS (APCI) *m/z* ([isotope], %) 931.1 (M⁺, [279Br], 90), 932.2 (M⁺ [281Br], 100), 933.2 (M⁺ [281Br], 57).

BisDBA Precursor 34. Diyne **33**^{1b} (478 mg, 1.15 mmol) was coupled to tetrayne **32** (446 mg, 0.48 mmol) by using general procedure D to yield **34** (555 mg, 73%) as an amorphous yellow solid. ¹H NMR (CDCl₃, 500 MHz) δ 7.72, (s, 1H), 7.68 (s, 1H), 7.63 (d, 2H, *J* = 8.0 Hz), 7.44 (d, 2H, *J* = 8.0 Hz), 7.27 (d, 2H, *J* = 7.0 Hz), 6.72 (d, 2H, *J* = 2.5 Hz), 6.48 (dd, 2H, *J* = 7.0, 2.5 Hz), 3.27 (t, 8H, *J* = 7.0 Hz), 1.56 (m, 8H, *J* = 7.5 Hz), 1.35 (m, 8H, *J* = 7.5 Hz), 0.96 (t, 12H, *J* = 7.5 Hz). ¹³C NMR (CDCl₃) δ 148.0, 135.4, 135.2, 133.8, 133.5, 133.3, 129.7, 129.5, 127.4, 127.1, 126.6, 124.5, 123.6, 115.4, 111.9, 111.6, 111.3, 106.5, 103.9, 97.8,

96.6, 94.3, 93.8, 92.2, 88.6, 50.8, 29.5, 20.5, 18.9, 14.2, 11.6, 11.5. IR (NaCl) ν 2961, 2945, 2885, 2863, 2198, 2150, 1591, 1509, 1470, 1392, 1363, 1322, 1249, 1170, 1132, 1094, 1068 cm^{-1} . HRMS (EI) for $\text{C}_{100}\text{H}_{134}\text{F}_6\text{N}_2\text{Si}_4$ $[\text{M}]^+$ calcd 1588.9523, found 1588.9518. MS (APCI) m/z ([isotope], %) 1588.6 (M^+ , 80), 1589.7 (M^+ [^{13}C], 100), 1590.8 (M^+ [^{213}C], 91). UV (CH_2Cl_2) λ_{max} (log ϵ) 315 (4.84), 422 (4.62). Em λ_{max} 533.

BisDBA 17. Octayne **34** (220 mg, 0.138 mmol) was cyclized by using general procedure E to yield **17** (82 mg, 62%) as a red solid. Mp 160–174 °C dec. ^1H NMR (CDCl_3) δ 8.34 (s, 1H), 8.27 (s, 1H), 8.03 (d, 2H, $J = 7.8$ Hz), 7.83 (s, 2H), 7.75 (d, 2H, $J = 7.8$ Hz), 7.69 (d, 2H, $J = 8.7$ Hz), 6.78 (s, 2H), 6.76 (d, 2H, $J = 8.7$ Hz), 3.33 (t, 8H, $J = 7.8$ Hz), 1.62 (m, 8H, $J = 6$ Hz), 1.40 (m, 8H, $J = 7.8$ Hz), 1.00 (t, 12H, $J = 7.5$ Hz). ^{13}C NMR (CDCl_3 , 500 MHz) δ 148.0, 134.9, 133.6, 132.8, 129.7, 129.5, 126.3, 126.1, 125.0, 124.0, 123.5, 122.7, 119.9, 115.3, 112.9, 111.5, 111.2, 97.7, 96.1, 93.0, 91.5, 87.9, 83.9, 82.0, 78.9, 51.0, 29.5, 20.6, 14.3. IR (NaCl) ν 2958, 2931, 2876, 2186, 2168, 1599, 1531, 1510, 1497, 1456, 1369, 1342, 1315, 1172, 1129 cm^{-1} . HRMS (EI) for $\text{C}_{64}\text{H}_{50}\text{F}_6\text{N}_2$ $[\text{M}]^+$ calcd 960.3873, found 960.3865. MS (APCI) m/z ([isotope], %) 960.2 (M^+ , 100), 961.2 (M^+ [^{13}C], 87), 962.3 (M^+ [^{213}C], 25). UV (CH_2Cl_2) λ_{max} (log ϵ) 322 (4.86), 454 (4.68). Em λ_{max} 544.

BisDBA 20. Octayne **34** (220 mg, 0.138 mmol) was cyclized by using general procedure F to yield **20** (77 mg, 58%) as a yellow solid. Mp 160–170 °C dec. ^1H NMR (CDCl_3) δ 8.64 (s, 1H), 8.25

(s, 1H), 7.75 (s, 2H), 7.62 (d, 2H, $J = 8.1$ Hz), 7.54 (d, 2H, $J = 8.1$ Hz), 7.37 (d, 2H, $J = 9.3$ Hz), 6.78 (s, 2H), 6.58 (d, 2H, $J = 9.3$ Hz), 3.28 (t, 8H, $J = 6.6$ Hz), 1.59 (m, 8H), 1.38 (m, 8H, $J = 7.5$ Hz), 0.99 (t, 12H, $J = 7.2$ Hz). ^{13}C NMR (CDCl_3 , 500 MHz) δ 148.0, 131.7, 131.3, 130.5, 129.7, 129.5, 129.4, 127.7, 126.9, 125.6, 124.8, 122.5, 120.3, 119.5, 115.0, 112.8, 112.2, 99.0, 98.5, 94.2, 93.1, 83.2, 81.9, 79.5, 77.5, 50.9, 29.5, 20.5, 14.2. IR (NaCl) ν 2957, 2932, 2871, 2183, 1593, 1531, 1328, 1292, 1169, 1119, 1063 cm^{-1} . UV (CH_2Cl_2) λ_{max} (log ϵ) 310 (5.17), 441 (4.92), 466 (4.95). Em λ_{max} 551. HRMS (ESI) for $\text{C}_{64}\text{H}_{50}\text{F}_6\text{N}_2$ $[\text{M} + \text{H}]^+$ calcd 961.3951, found 961.3951. MS (APCI) m/z ([isotope], %) 960.3 (M^+ , 92), 961.1 (M^+ [^{13}C], 100), 962.5 (M^+ [^{213}C], 12).

Acknowledgment. We thank the National Science Foundation (CHE-0718242) for financial support. E.L.S. acknowledges the NSF for an IGERT fellowship (DGE-0549503). We thank Ben Boal and Zack Mensinger for preparation and characterization of selected precursor molecules.

Supporting Information Available: Experimental details, copies of NMR spectra for new compounds, and additional self-association data. This material is available free of charge via the Internet at <http://pubs.acs.org>.

JO701740N